

Design and modal analysis of dual-slot circular patch antenna for ultra-wideband applications

K. JAGADEESH BABU^{1*}, RABAH W. ALDHAHERI², L. SIVA SAI¹, BHASKARA RAO PERLI¹, TATHABABU ADDEPALLI³, SRINIVASA RAO PASUMARTHI¹, B. KIRAN KUMAR¹, V. N. KOTESWARA RAO DEVANA³

¹Department of ECE, St. Ann's College of Engineering & Technology(A), Chirala, AP, India

²Department of Electrical and Computer Engineering, King Abdulaziz University, Jeddah 21589, Saudi Arabia

³Department of ECE, Aditya Engineering College (A), Surampalem, Kakinada, AP, India

A novel and high performance UWB antenna is designed in the present work. The proposed antenna consists of a slotted circular disk with Defected Ground Structure (DGS). The rectangular and bevel-shaped slots are inserted in the circular radiating patch and on the top edge of the partial ground plane, respectively, to change the mode behavior and exhibit multiple resonance modes. Characteristic Mode Analysis (CMA) is the latest emerging technique in understanding the radiation phenomena of the antenna. The developed antenna is analysed by using CMA and various modal parameters like characteristic angle, modal significance and modal patterns are used to study the performance of the antenna for wideband operation and stable radiation pattern. The antenna has the low-profile structure and small dimension of $38 \times 35 \times 1.6 \text{ mm}^3$ giving an impedance bandwidth ranging from 2.47 to 14.31 GHz for Voltage Standing Wave Ratio (VSWR) < 2 and a maximum gain of 3.9 dBi and a maximum radiation efficiency of 90%. Within its operating band, the antenna exhibits stable radiation patterns. The simulated and measured results of the proposed antenna are in good agreement.

(Received September 15, 2021; accepted August 10, 2022)

Keywords: Ultra-wideband (UWB), Monopole, CMA, Radiation pattern, Modal currents

1. Introduction

The present advanced wireless applications demand antennas with low power and wideband operating capabilities. The antennas covering the band 3.1 to 10.6 GHz known as UWB antennas meet these requirements [1]. The power levels in UWB are restricted to -41.3 dBm/MHz for wireless applications. Also, the operational bandwidth for UWB technology is defined to be 7.5 GHz. The significant features of UWB are low power handling capability, feasibility to higher data rates for short distance communications at lower implementation costs. In addition, UWB is a vibrant technology with numerous applications such as in high-resolution ground-penetrating radar, vehicular radars, short-range high-speed data communications and measurement systems [2]. UWB antennas should be lightweight, low profile and very compact to fit into the portable devices such as wireless media players, mobile phones, wireless storage devices, digital cameras and so on. Planar monopole antennas are the good choice for satisfying the requirements of UWB system for use in portable devices owing to the planar and simple structure [3].

The main challenge in the design of UWB antennas is achieving low profile with stable radiation patterns. Most of the UWB antennas are planar monopole antennas owing to their ease of fabrication, planar like structure and wideband properties. Defected ground plane, orientation of the patch and size of the antenna are significant factors in attaining the UWB band of frequency during the antenna

design process. UWB antennas with various shapes like circular, square, rectangular, inserted arc-shape etc are presented in the literature [4]. In order to obtain wideband properties, various techniques are used in the literature, such as truncated slots, defective ground structures, changing the radiating patch, introducing slots at the patch and ground plane, etc. [5]-[6].

In [7], a novel UWB MIMO antenna using decoupling structure was developed. In [8], the modified bow-tie-shaped vertical radiator worked well with the L-shaped and one inverted U-shaped combination. When the antenna's seven resonant modes are combined together, it can cover a wide range of frequencies, from 3.035 to 17.39 GHz. In [9], a novel method of UWB design using hybrid optimization method is presented. The method uses this optimization method for parametric tuning for getting UWB spectrum. In [10], a novel shape compact microstrip antenna for ultra-applications is presented. The developed antenna operates from 3.3 to 11.5 GHz giving a maximum gain of 1.4 dBi with omnidirectional radiation characteristics. A novel method of UWB antenna design using fractal structure is developed for microwave imaging in [11]. In [12], a novel UWB antenna with Defect Ground Structure (DGS) is proposed for wireless applications. These antennas achieve a wide impedance bandwidth, good gain, and a stable radiation pattern, but they do not focus on providing the underlying physical insights required to generate ultra-wideband.

In this work, a novel dual-slot circular disk monopole antenna with Defected Ground Structure (DGS) giving

UWB operation is introduced. The main novelty of the work is the analysis of proposed antenna to get stable radiation patterns using CMA technique. Various antenna parameters like VSWR (Voltage Standing Wave Ratio), reflection coefficient, and radiation pattern are obtained to analyse and predict the operation of the proposed antenna. Also, CMA method is used in characterising the performance of the antenna.

2. Antenna design

In the design process of antenna, FR-4 substrate with a dielectric constant value of 4.3, a thickness of 1.6 mm and a loss tangent of 0.002 is utilized. The dimensions of the antenna are $38 \times 35 \times 1.6 \text{ mm}^3$. The proposed antenna operating in UWB band is presented in Fig.1. In the initial design process, a circular slot is taken on the substrate and two rectangular slots are inserted on the disk to give UWB characteristics as shown in the Fig. 1(a). A microstrip line with dimensions L_f and W_f is used to feed the antenna. A bevel-shaped slot on the ground plane acting as DGS is shown in Fig. 1(b). This DGS is crucial in giving the UWB performance of the antenna.

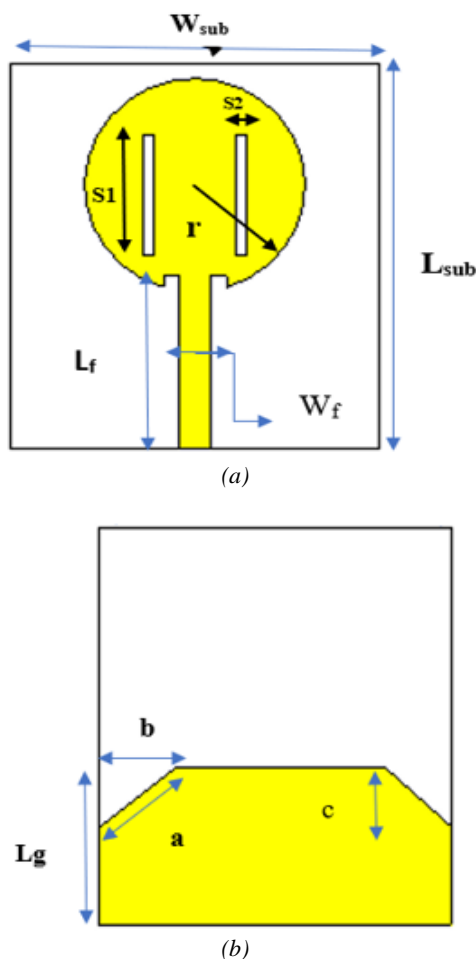


Fig. 1. Proposed UWB antenna (a) Front View (b) Back View (color online)

The radius an of the circular patch is calculated using the equations below [13]

$$a = \frac{F}{\left\{ 1 + \frac{2h}{\pi \epsilon_r F} \left[\ln \left(\frac{\pi F}{2h} \right) + 1.7726 \right] \right\}^{1/2}} \quad (1)$$

where,

$$F = \frac{8.791 \times 10^9}{f_r \sqrt{\epsilon_r}} \quad (2)$$

The electrical length of the rectangular-shaped slot can be defined at a given centre frequency f_c as follows [14]:

$$L_{\text{slot}} = \frac{c}{2 * f_r \sqrt{\frac{\epsilon_r + 1}{2}}} \quad (3)$$

where ϵ_r the relative permittivity of the substrate and c is the velocity of light in free space.

Initially, a disk of radius 10.5 mm is taken on an FR4 substrate with permittivity value 4.3 having thickness 1.6 mm in the design process of the antenna. The antenna is fed with a 50Ω microstrip feed line. The width of the feed is taken as 3 mm and its length is taken as 18 mm. Further, two rectangular slots are introduced on the circular disk to give UWB band of operation. The ground plane is taken with Perfect Electric Conductor (PEC). To give wideband characteristics, the ground plane is partially removed. Bevels shaped slots are introduced on the ground plane to further improve the design and thus to obtain UWB band. The important dimensions of the designed antenna are shown in Table 1. All the values are finalized after performing parametric analysis to give desired UWB characteristics.

Table 1. Dimensions of the proposed antenna

Parameter	Description	Value(mm)
L_{sub}	Length of the Substrate	38
W_{sub}	Width of the Substrate	35
r	Diameter of Circular disk	10.5
L_f	Length of the Patch	18
W_f	Width of the Patch	3
a	Length of the Bevel	7
b	Width of the Bevel	7
c	Height of the Bevel	7
L_g	Length of the Ground Plane	15
S1	Length of the Slot	12
S2	Width of the Slot	1

2.1. Parametric analysis

The diameter of the circular disk, 'r' and the ground dimension 'b', 'c' and patch slot play a key role in obtaining the wideband characteristics. This section introduces the parameter analysis for optimizing these parameters. In the first step, for different values of the diameter of the disc, $r = 10$ mm, 10.5 mm, and 11 mm, the parameter analysis is performed as shown in Fig. 2.

In the second step, parametric analysis is performed for dimensions of the ground plane such as height of the bevel 'c' and the bevel width, 'b', slot length 'S1' and width of the slot 'S2'. It is observed from Fig. 3 and Fig. 4 that a wide impedance bandwidth from 2.47 to 14.31 GHz is achieved for the bevel dimensions $c = 7$ mm, and $b = 7$ mm. In the next step, parametric analysis is performed for dimensions of the patch slot, viz: length of the slot, 'S1' and width of the slot, 'S2'. It is observed from Fig. 5 and Fig. 6 that a wide impedance bandwidth from 2.47 to 14.31 GHz can be achieved for the slot dimensions $S1 = 12$ mm, and $S2 = 1$ mm. The variation of reflection coefficient with full ground plane, reduced ground plane and bevel-shaped ground plane are shown in Fig. 7(a), from which it is observed that bevel cut on the ground plane plays significant role in achieving wide impedance bandwidth. The wide impedance bandwidth of the reconfigured circular-shaped slot antenna is described as follows: Because the input impedance is a function of the antenna's geometry, dimensions, and feeding configuration, the antenna's impedance bandwidth is usually achieved by its difference from the standard 50 ohm. By modifying the ground structure and inserting slots into the radiating patch, an impedance matching network is created. As illustrated in Fig. 7(b), the impedance of the proposed design approaches the standard 50 Ohm characteristic impedance.

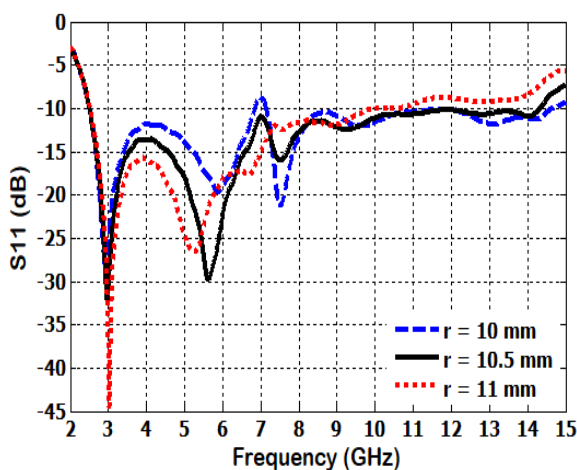


Fig. 2. Parametric analysis of S_{11} w.r.t. diameter of circular disk (color online)

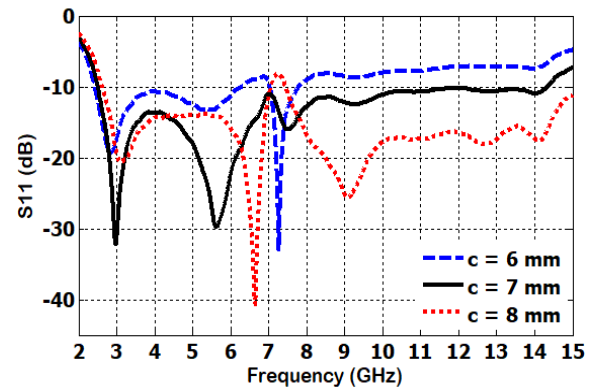


Fig. 3. Parametric analysis of S_{11} w.r.t. height of the bevel 'c' (color online)

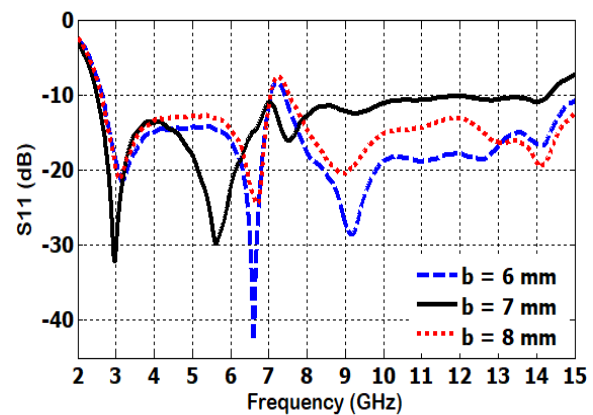


Fig. 4. Parametric analysis of S_{11} w.r.t. width of the bevel 'b' (color online)

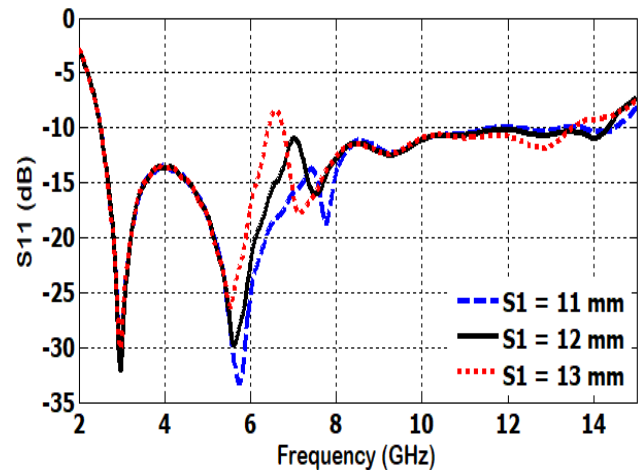


Fig. 5. Parametric analysis of S_{11} w.r.t. length of the slot $S1$ (color online)

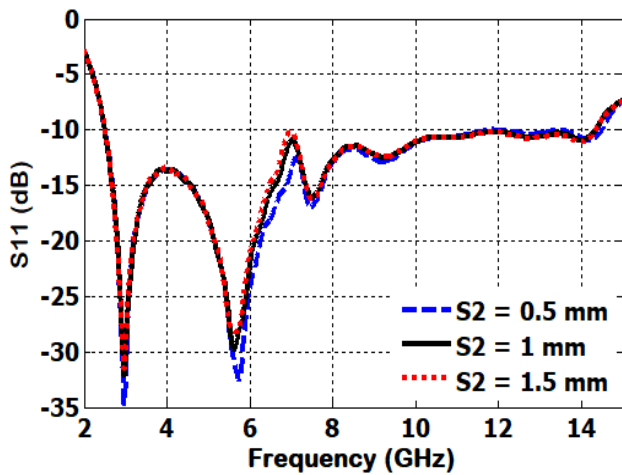
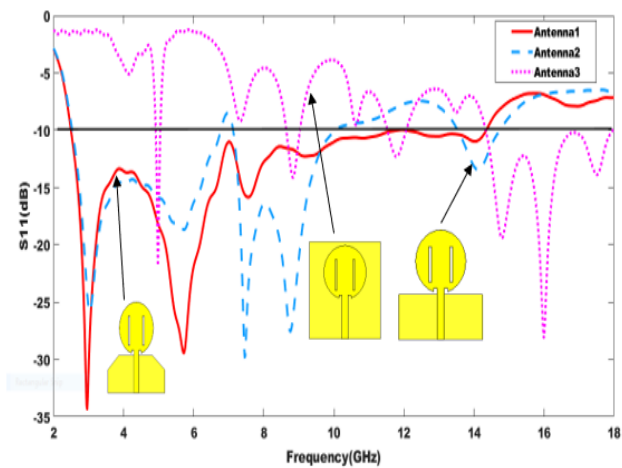
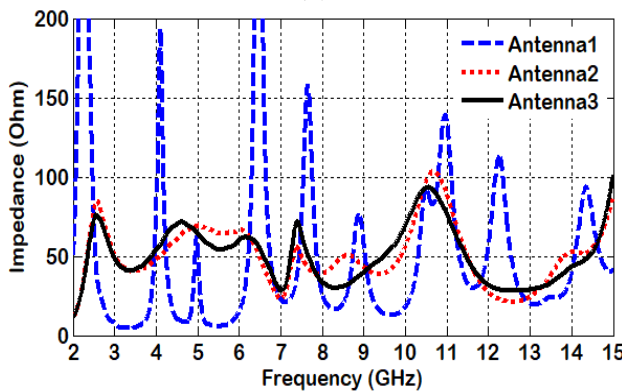


Fig. 6. Parametric analysis of S_{11} w.r.t. width of the slot S_2 (color online)



(a)



(b)

Fig. 7. S_{11} variation (a) and Z parameters (b) for various configurations of the circular-shaped slot antenna (color online)

2.2. Design Procedure using CMA

TCM involves the generation of orthogonal surface currents of the radiating conductor, which are known as modes. According Garbacz [15], infinite number of modes can be generated for any conductor and these modes

decide the radiation mechanism of the antenna. Later, it is further elaborated by method of moment matrix by Harrington [16,17]. These modes depend on the size and shape of the radiator and not on the excitation [18,19]. CMA method can be effectively utilized in arriving at the physics of the antenna radiation mechanism, which will be useful in exactly predicting the radiation properties of the antenna [20-23].

Usually, modal patterns and modal currents are used in studying the physics of the radiating structure. The intrinsic relation between modal current and impedance matrix is given in Eq.(1) [16].

$$X(J_n) = \lambda_n R(J_n) \tag{1}$$

where, R and X are the real and imaginary values of impedance matrix; λ_n values are known as eigen values and J_n are known as surface currents. λ_n values range from $-\infty$ to $+\infty$. The values corresponding to $\lambda_n = 0$ are taken as resonant frequencies and other values represents the energy stored in electrical or magnetic fields. Modal Significance (MS) is another important parameter in the analysis of radiation mechanism of the antenna, which is related to eigen values as specified in Eq. (2).

$$MS = |1/1 + j \lambda_n| \tag{2}$$

Another important parameter in locating the resonant frequency of the radiating structure is Characteristic angle α_n , which is related to eigen values as mentioned in Eq.(3) and these values of α_n equal to near to 180° corresponds to the radiating bandwidth of the conductor.

$$\alpha_n = 180^\circ - \tan^{-1}(\lambda_n) \tag{3}$$

For circular disk, CMA is performed using the modal parameters; characteristic angle and modal significance as shown in Fig. 8 and Fig. 9. From characteristic angle values shown in Fig. 8, it is observed that none of the modes take 180° value at lower band of frequencies. This is clearly seen from MS curves shown in Fig. 9, from which also it is seen that at lower frequencies none of the MS curves touch '1' value and significant values are obtained at higher frequencies only. Therefore, it is not possible to obtain wideband characteristics. Hence, a method of introducing slots in the radiating patch is adopted.

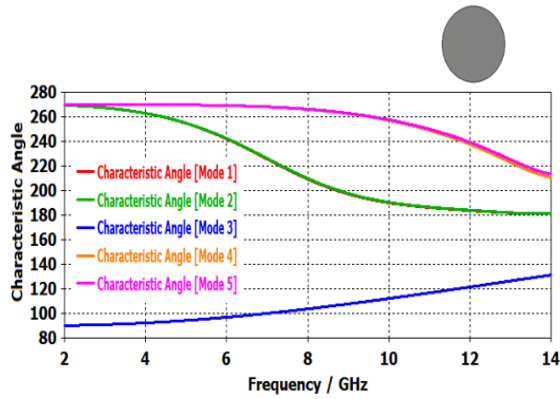


Fig. 8. Characteristic angle of circular disk (color online)

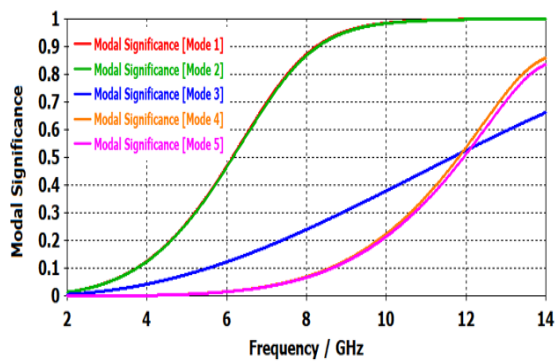


Fig. 9. Modal significance of circular disk (color online)

In the evolution process of wideband antenna, a slot is introduced on the left side of the patch and characteristic angle and modal significance plots are given as shown in Fig. 10 and Fig. 11 respectively. From characteristic angle values shown in Fig. 10, it is observed that mode 1 takes an 180° value at 7.2 GHz and the remaining modes do not cross the 180° value. From Fig. 11, it is seen that only mode 1 resonates at 7.2 GHz and contributing to the radiation in the UWB band and remaining modes resonate at beyond the frequency of interest. Therefore, it is not possible to get wideband characteristics and hence the circular patch is further modified.

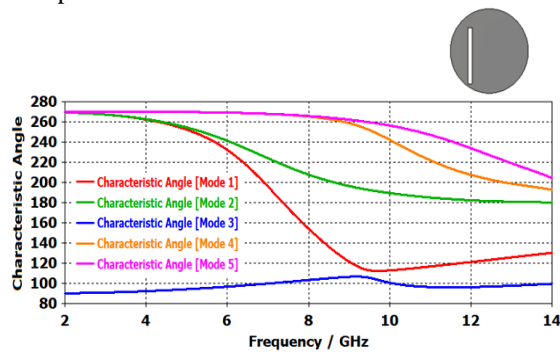


Fig. 10. Characteristic angle of circular disk with single slot (color online)

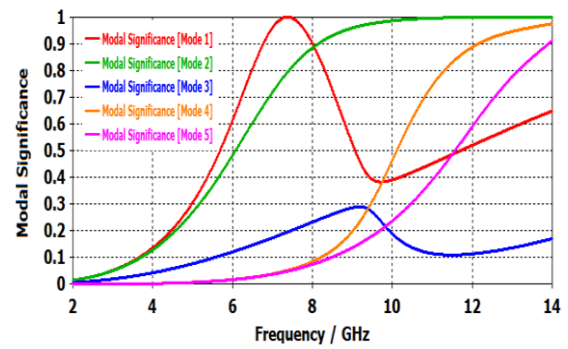


Fig. 11. Modal significance of circular disk with single slot (color online)

In the next step, one more slot is introduced on the circular patch and characteristic angle and modal significance values are obtained as shown in Fig. 12 and Fig. 13. From the characteristic angle values shown in Fig. 12, it is observed that modes 1 and 2 cross the 180° value at 6.8 GHz and 8.7 GHz, respectively, and the remaining modes do not cross the 180° value. From MS curves, it is observed that modes 1 and 2 resonate at 6.8 GHz and 8.7 GHz and both modes contribute to the radiation of the antenna in the desired UWB band and the remaining modes resonate beyond the frequency of interest. However, in order to obtain wide bandwidth that is 3.1-10.6 GHz, further modifications are applied on the ground plane.

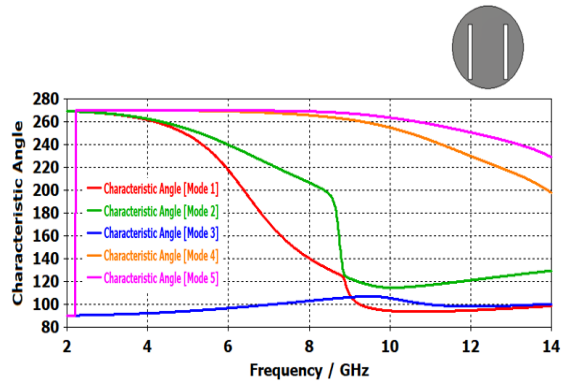


Fig. 12. Characteristic angle of circular disk with two slots (color online)

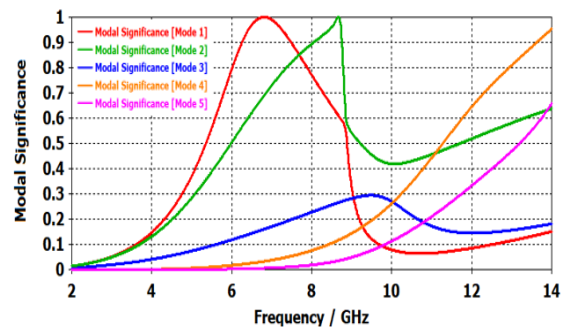


Fig. 13. Modal significance of circular disk with two slots (color online)

In addition to the slotted circular disk, the ground structure is cut in a bevel shape at the edges of the top surface as shown in Fig. 14. Due to DGS, modes 4 and 5 also resonate within the frequency of interest along with modes 1 and 2 as shown in Fig. 15. Therefore, modes 1, 2, 4, and 5 exhibit the wideband characteristics and contribute to the antenna for obtaining wide bandwidth. Mode 3 does not contribute to the antenna's radiation due to the insignificant MS values.

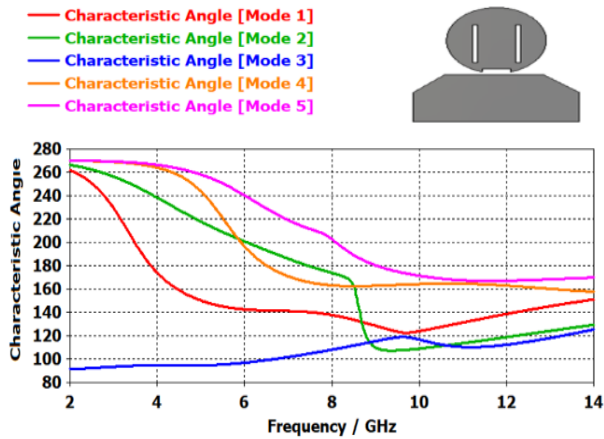


Fig. 14. Characteristic angle of proposed antenna (color online)

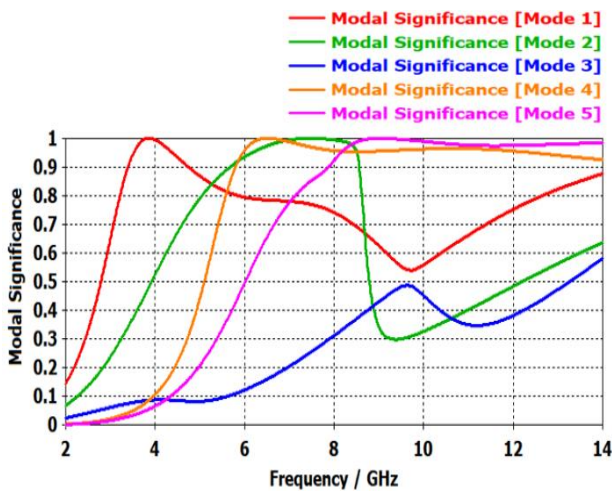


Fig. 15. Modal significance of proposed antenna (color online)

The surface current distribution on the circular patch for all the modes is shown in Fig. 16. It is observed from the modal currents that the maximum current distributions in modes 1, 2, 4, and 5 exist at the lower part of the patch hence feeding is applied at the same location so that modes 1, 2, 4, and 5 will be excited. Mode 3 is not useful since it does not cross 180° of characteristic angle in the desired band of interest. The modal patterns for all modes are plotted in Fig. 17, from which it is observed that the modes 2 and 4 give maximum boresight radiation and modes 1 and 5 also seem to give optimum radiation in the boresight direction. Hence, when the antenna is excited all modes combinedly give maximum and stable boresight

radiation, which is presented in the following in the following sub-section.

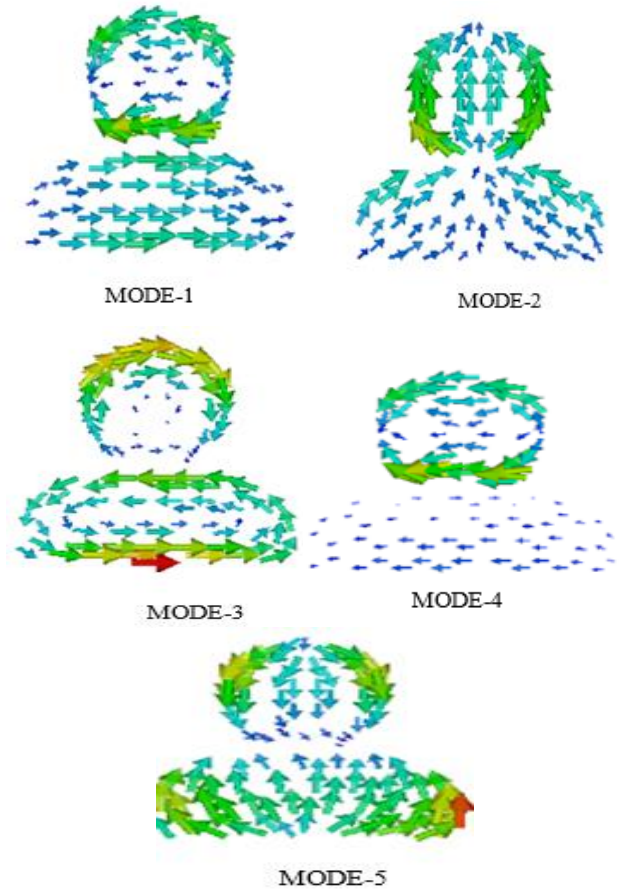


Fig. 16. Modal currents at five modes of proposed antenna

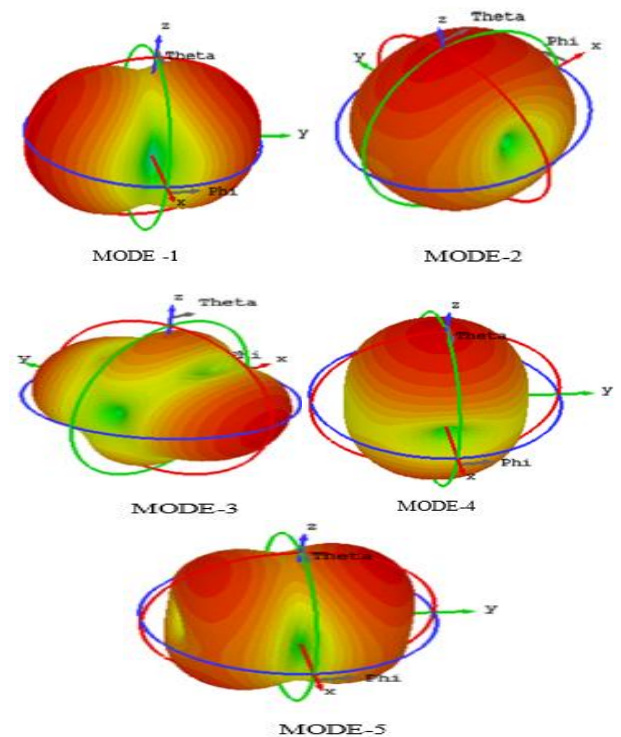


Fig. 17. Radiation patterns of proposed antenna (color online)

Based on CMA it is observed that the desired modes 1, 2, 4, and 5 of the proposed antenna have wideband characteristics, which is evident when observing the operating frequency bands of the desired modes in Table 2. The combined excitation of modes 1, 2, 4, and 5 of the antenna model with a suitable feed configuration can improve bandwidth for wideband antenna applications.

Table 2. Useful modes contributing for radiation

Mode	Operating frequency range based on $MS > 0.707$
Mode 1	2.2GHz to 2.9 GHz
Mode 2	2.7 GHz to 8.57GHz
Mode 4	4.2 GHz to 14.31 GHz
Mode 5	5.9 GHz to 14.31GHz.

3. Results and discussion

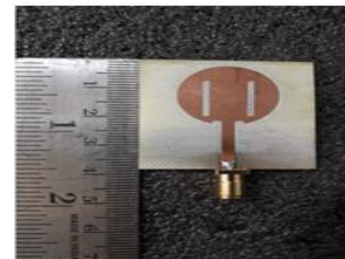
The fabricated prototype and S_{11} -parameters measurement setup is shown in Fig. 18. The simulated and measured reflection coefficient curves are shown in Fig. 19, which are found to be in good agreement. The proposed antenna covers the UWB band intended to be used for naval radar systems, satellite communications, RFID, WLAN applications as the antenna resonates at various band of frequencies viz: 3 GHz, 5.8 GHz and 7.5 GHz. The simulated and measured gain plot of the proposed antenna is shown in Fig. 20 (a), from which it is observed that the antenna gives a maximum gain around 4 dB. Similarly, the simulated and measured efficiency plots of the proposed antenna are given in Fig. 20 (b), showing a maximum efficiency of 90 % in the operating band.

The basic circular disk is only capable of producing frequencies in the multi-band range. The reason for this is that, according to the results of the modal analysis of the circular disk, the resonant frequencies of characteristic modes are not sufficiently close. The corresponding modes are moved closer to each other by increasing the electrical current path of the modes by inserting two rectangular slots into the circular disk. In addition, on the partial ground plane, bevel-shaped slots are introduced for the resonant frequencies of the modes that move close enough together. By properly exciting these modes, this type of modal behavior contributes to the generation of the UWB band.

The proposed approach for achieving a wide frequency range of the antenna is described with help of 2D-surface current distribution, as shown in Fig. 21. Fig. 21 (a)–(d) depict surface current distributions at frequencies of 3, 5.6, 7.5, and 9.3 GHz, with respect to first, second, third, and fourth order harmonics. The surface currents are mostly concentrated on the sides of the radiator, around the slots, and the ground structure, as shown in Fig. 21. The current continues to flow from the radiator through the feed line to the top edges of the ground structure, and the radiator transmits electromagnetic wave into free space. Surface currents on the bottom surface of the radiating patch are strongly

coupled to the top surface of the ground structure near the feed line which is contact to the radiator, resulting in the proposed antenna having a wide operating bandwidth.

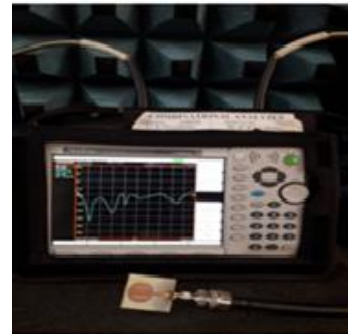
The measured E-plane and H-plane radiation patterns of the antenna at 3, 5.8, and 7.5 GHz are shown in Fig. 22. The radiation pattern of the proposed antenna exhibits omnidirectional and figure-of-eight shapes in the E-plane and H-planes respectively. In the entire band of interest the antenna is shown to exhibit stable radiation pattern as mentioned in the earlier sub-section due to the excitation of modes 1, 2, 4 and 5. The stable radiation pattern of the proposed antenna provides good radiation performance in the frequency range of interest and is the main significant outcome of the proposed work.



(a)



(b)



(c)

Fig. 18. Prototype of the fabricated antenna (a) Top view and (b) Bottom view and (c) S_{11} , measurement setup (color online)

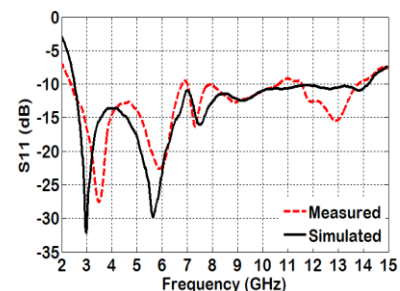


Fig. 19. Simulated and measured S_{11} parameters of proposed antenna (color online)

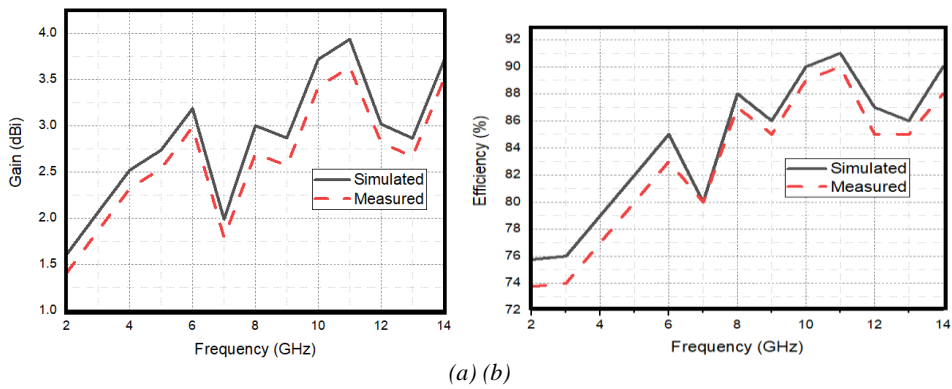
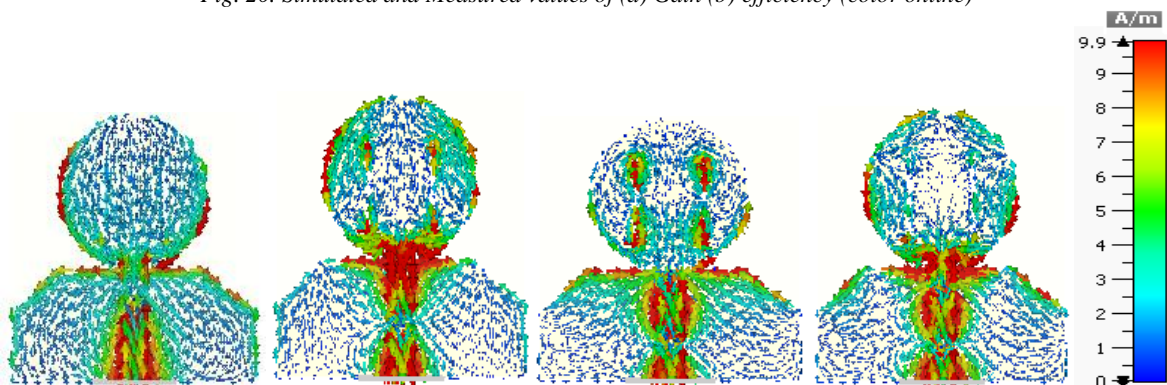


Fig. 20. Simulated and Measured values of (a) Gain (b) efficiency (color online)



(a) (b) (c) (d)

Fig. 21. Surface current distributions at (a) 3 GHz, (b) 5.6 GHz, (c) 7.5 GHz, and (d) 9.3 GHz (color online)

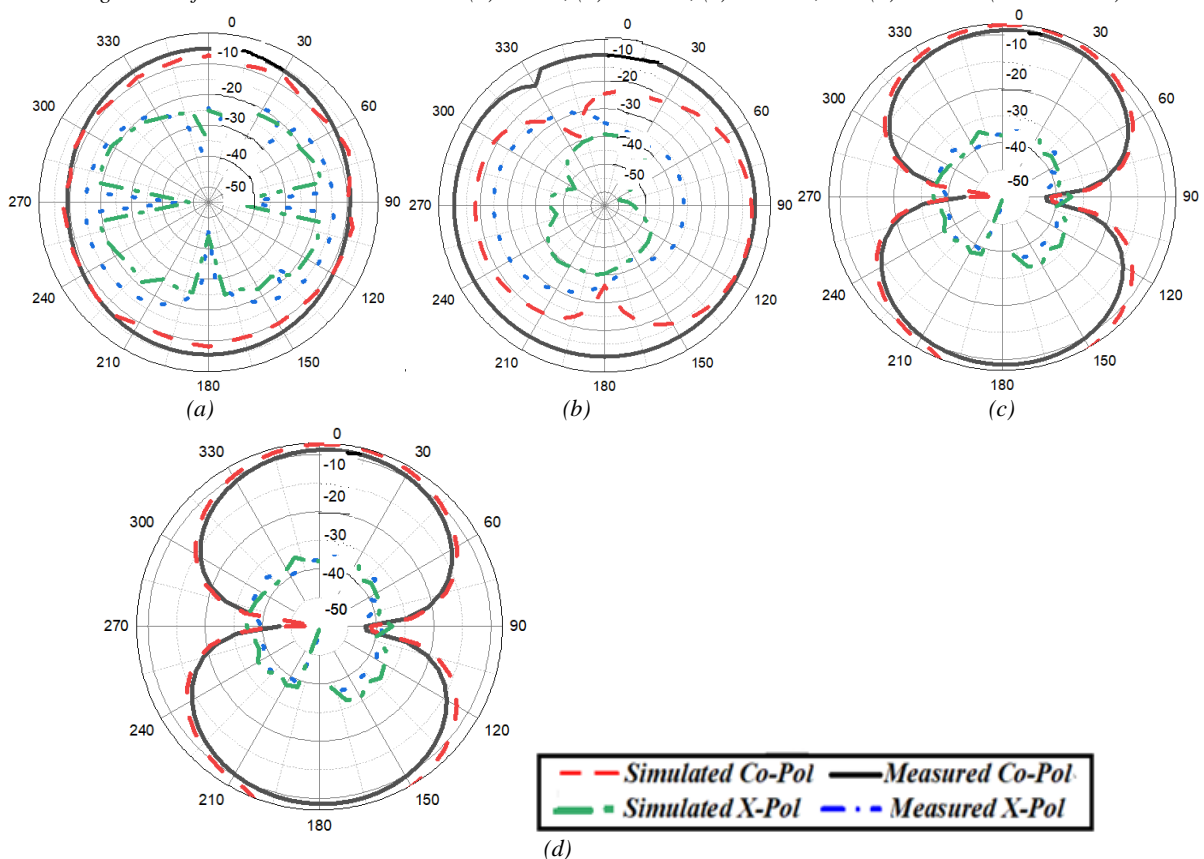


Fig. 22. Radiation pattern of proposed antenna at (a) E-Plane at 5 GHz (b) H-Plane at 5 GHz (c) E-Plane at 9 GHz (d) H-Plane at 9 GHz (color online)

Table 3. Comparison with existing work

Ref.	Size (mm × mm)	Overall Size (mm ³)	Operating band (GHz)	Peak Gain (dBi)
[7]	35 × 25	875	3 to 11	3.0
[8]	24.5 × 20	784	3.035 to 17.39	4.56
[10]	14 × 18	403.2	3.3 to 11.5	1.4
[24]	60 × 58	5,568	3.4 to 10.2	3.18
[25]	29 × 39	1,436	2.9 to 15.9	----
[26]	66 × 62	4,092	2.4 to 12	5
[27]	30 × 30	900	2.8 to 12	----
[28]	26 × 28	1,164.8	3.7 to 18	3.97
[29]	25 × 17	680	2.97 – 22.46	3.07
[30]	18 × 25	720	2.8–17	5.38
Proposed	38 × 35	2,128	2.47 to 14.31	3.9

4. Conclusion

The proposed antenna has a low-profile structure and a compact size of $38 \times 35 \times 1.6$ mm³, giving an impedance bandwidth of 2.47 to 14.31 GHz, a maximum gain of 3.9 dBi, a maximum radiation efficiency of 90% and stable radiation patterns on both the E- and H-planes, making it suitable for current UWB wireless applications. The wideband performance of the antenna is obtained by introducing slots on the patch and modifications in the ground plane. CMA method is effectively implemented in the design of the proposed antenna to characterize the radiation performance of the antenna by studying the parameters like modal patterns, modal significance and characteristic angle.

References

- [1] H. Schantz, The art and science of UWB antennas, Artech House, Norwood, MA, 2005.
- [2] Q. Wu, R. Jin, J. Geng, M. Ding, IEEE Trans Antennas Propag. **56**, 896 (2008).
- [3] K. G. Thomas, M. Sreenivasan, Electron. Lett. **45**, 445 (2009).
- [4] K. Jagadeesh Babu, B. Kiran Kumar, Subba Rao Boddu, A. M. Varapasad, International Journal of Electronics Letters **7**(4), 448 (2019)
- [5] D. Valderas, J. Melendez, I. Sancho, Microwave Opt. Technol. Lett. **46**, 6 (2005).
- [6] Rabah W. Aldhaheeri, Kamili Jagadeesh Babu, Avez Syed, Muntasir M. Sheikh, Microwave and Optical Technology Letters **57**(10), (2015)
- [7] L. Wang, Z. Du, H. Yang, R. Ma, Y. Zhao, X. Cui, X. Xi, X IEEE Antennas and Wireless Propagation Letters **18**(8), 1641 (2019).
- [8] R. Azim, M. T. Islam, H. Arshad, M. M. Alam, N. Sobahi, A. I. Khan, IEEE Access **9**, 5343 (2021).
- [9] P. Kumar, S. Shilpi, A. Kanungo, Varun Gupta, Neeraj Kumar Gupta, Wireless Personal Communications **122**, 1129 (2022).
- [10] Saad Hassan Kiani, Xin Cheng Ren, Muhammad Rizwan Anjum, Khalid Mahmood, Haider Ali, Naveed Jan, Muhammad Adil Bashir, Muhammad Abbas Khan, International Journal of Antennas and Propagation, 2021, 1(2021).
- [11] H. M. Q. Rasheda, Norsaliza Abdullah, Qazwan Abdullah, Nabil Farah, Abbas Uğurenver, Abdul Rashid O. Mumin, Adeb Salh, 2021 International Congress of Advanced Technology and Engineering (ICOTEN), 1 (2021)
- [12] K. Karthika, C. Kavitha, K. Kavitha, B. Thaseen, G. Anusha, E. Nithyaanandhan, 2020 International Conference on Inventive Computation Technologies (ICICT), 937 (2020).
- [13] C. A. Balanis, Antenna Theory: Analysis and Design, 3rd edition, Wiley, New York, NY, USA, 2005.
- [14] A. M. Abbosh, M. E. Bialkowski, IEEE Transaction on Antennas and Propagation **57**(3), 796 (2009).
- [15] R. J. Garbacz, R. H. Turpin, IEEE Transactions on Antennas and Propagation **19**(3), 348 (1971)
- [16] R. F. Harrington, J. R. Mautz, IEEE Transactions on Antennas and Propagation **19**(5), 622 (1971).
- [17] R. F. Harrington, J. R. Mautz, IEEE Transactions on Antennas and Propagation **19**(5), 629 (1971).
- [18] B. K. Lau, D. Manteuffel, H. Arai, S. V. Hum, IEEE Transactions on Antennas and Propagation **64**(7), 2590 (2016)
- [19] M. Vogel, G. Gampala, D. Ludick, C. J. Reddy, IEEE Antennas and Propagation Magazine **57**(2), 307 (2015)
- [20] Weiwen Li, Yongcong Liu, Jie Li, Longfang Ye, Qing Huo Liu, International Journal of Antennas and Propagation, 1 (2019)
- [21] J. B. Kamili, A. Bhattacharya, Proceedings of 2019 IEEE Region 10 Conference (TENCON), Kochi, India, 1903 (2019).
- [22] K. J. Babu, L. S. Sai, G. Divya, Y. T. Mohammed, M. A. Hussaini. Telecommunications and Radio Engineering **79**, 13 (2020).
- [23] P. K. Gentner, 2020 14th European Conference on Antennas and Propagation (EuCAP), 1 (2020),
- [24] L. Sumana, Esther Florence Sundarsingh, S. Priyadarshini, IEEE Transactions on Components, Packaging and Manufacturing Technology **11**(1), 3 (2020).
- [25] Luz I. Balderas, Alberto Reyna, Marco A. Panduro, Carlos Del Rio, Arnulfo R. Gutiérrez, IEEE Access **7**, 127486 (2019).
- [26] Kamla Prasan Ray, Sanjay Singh Thakur, Wireless Personal Communications **109**(3), 1689 (2019).
- [27] Adamu Halilu Jabire, Anas Abdu, Salisu Sani, Sani Saminu, Aliu Uba Taura, Mohammed Olatunji Obalolu, Elekrika-Journal of Electrical Engineering **18**(3), 34 (2019).
- [28] L. Liu, S. W. Cheung, R. Azim, M. T. Islam, Microwave and Optical Technology Letters **53**(10),

2283 (2011).

[29] Rakesh N. Tiwari, Prabhakar Singh,
Binod Kumar Kanaujia, AEU-International Journal of
Electronics and Communications **104**, 58 (2019).

[30] Rakesh Nath Tiwari, Prabhakar Singh,
Binod Kumar Kanaujia, Amit Kant Pandit, Wireless
Personal Communications **114**(4), 3031 (2020).

*Corresponding author: jagan_ec@yahoo.com